Journal of Pressure Equipment and Systems 2 (2004) 79-85

Stress corrosion cracking as evolving interface problem

Andrey P. Jivkov *

Corrosion and Protection Centre, UMIST, Sackville Street, P.O. BOX 88, Manchester M60 1QD, UK

Abstract

It has been long recognised that stress corrosion crack initiation and propagation are triggered by the interaction between electro-chemical processes and mechanical deformation in the crack tip region. Recently, the author of the present work proposed a model for corrosion crack nucleation and growth, which allows for incorporation in a continuum mechanical theory. In the model, the corrosion is forming the geometry of the crack tip, thus creating the conditions for strain concentration. This leads to a smooth crack surface evolution represented as a problem of evolving interface, where crack growth criterion is not needed. As a start, the chemical environment of the crack tip is assumed to be constant and unaffected by the changing geometry as the crack is developing. This leads to a linear relationship between strain and corrosion rate, in the sense of removed material per unit of area. This work reviews the results obtained so far on the basis of the linear model. In addition, mathematical and finite element analyses of stationary cracks with appropriate geometry are involved to explain the behaviour predicted by the model.

Keywords: Stress corrosion cracking; Crack initiation; Crack evolution; Crack tip geometry; Moving boundaries.

1. Introduction

The phenomenon of stress corrosion cracking (SCC) has been intensively studied during the last three decades. The motivation is that SCC is a cause for many failures of structures operating under loads significantly lower than the design ones. Corrosion is associated with two major processes operating at the metal-solution interface–metal dissolution and passive film formation. The dissolution process is in fact loss of metal atoms from the surface to the environment and is the major deterioration mechanism. In contrast, the passive film that many metal surfaces form in aqueous solutions (typically of thickness 1-10 nm) inhibits the dissolution to a great extent: dissolution rate may become several orders of magnitude lower than the rate under bare metal conditions [1]. Failures of the passive film at various positions may, however, occur due to changes in electrochemical conditions in the environment, or as a result of mechanical damage. As the film fails in some surface region, the rate of dissolution may increase to the rate at bare surface conditions, resulting in a (comparatively) rapid material loss.

Two specific complexities arise in the case of SCC. The first concerns the localised electrochemical conditions that exist inside a growing crack. These may significantly differ from the bulk chemistry, which means that the conditions under which the corrosion processes operate inside the crack are not the same as those that can be measured on the external solid surface. The bulk of research on SCC has been focused on this problem. Existing models account to various extent for the electrochemical, chemical and transport processes in the environment and predict to various extent of accuracy the steady-state solution chemistry and electrode kinetics in the crack tip vicinity [2-4].

The second complexity in SCC arises from the synergy between the dissolution/passivation processes and the deformation (straining) of the solid due to mechanical loading. One widely used hypothesis for SCC is that of anodic dissolution localized at the surface region where the metal is exposed and experiences the highest strains [5]. In the models for SCC based on anodic dissolution, e.g. [2, 6], the passive film is considered to be intact along the crack surface and to rupture in a cyclic manner but only in a relatively small region of sufficiently large strains. From a fracture mechanical perspective, the active region in these models is only the crack tip, i.e. geometrically a point. Hence, the mechanical description is based on a single parameter, e.g. the strain energy release rate during crack growth and as a consequence all details, such as stresses, strains, displacements, are uniquely controlled by the chosen parameter, see e.g. [7]. For this reason the anodic dissolution models for SCC are not actually concerned with the synergy between the surface deformation and the corrosion, although the key role of this interaction has long been recognised.

Classical fracture mechanics considers cracks with ideal geometries, i.e. they are thought of as slits with atomically sharp end(s) or tip(s). This is justified when they are viewed on sufficiently large scale. Micrographs of corrosion cracks, however, show that

* Corresponding author.
E-mail address: andrey.jivkov@ts.mah.se (Andrey P. Jivkov).

their near-tip regions are smooth integral parts of the crack surface, very much like plastically blunted tips, see e.g. [8]. This allows a continuum mechanical formulation of the problem, where crack propagation means evolution of the solid surface (or solid-solution interface) with time.

A preliminary model for propagation of such realistic cracks, based on anodic dissolution as deterioration process, has been proposed in [9]. The passive film is considered as a dimensionless brittle scale covering the metal surface and a simple physical argument for strain-induced rupture of the film leads to a linear relation between the surface evolution rate and the surface strain. The results show that the local geometry at the crack tip has a significant influence on the growth rate and that two major length parameters control this influence – the crack width and the radius of curvature at the tip. The local geometry control could explain some of the scatter in the stress corrosion crack growth rates that have been observed during experiments under identical bulk electrochemical and loading conditions [10].

Despite its simplicity, the model from [9] demonstrates the key role of the deformation-corrosion interaction, which becomes even more pronounced when studying the early stages of corrosion crack evolution. The history of a corrosion crack is followed from the formation of a pit on a practically smooth solid surface, through the nucleation of a crack from the pit, to the propagation of the shaped crack [11,12]. A key result is that the geometry of the realistic crack formed controls the crack behaviour during incubation and short growth, as for long cracks in [9]. The present work reviews the results obtained so far on the base of the linear model. It is the geometry of the evolving crack that is of a concern in this study, and the time dimension of the evolution is intentionally avoided. Mathematical analysis and finite element results for stationary cracks with appropriate realistic geometry are then used to explain the observed geometry evolution.

2. Evolution problems and results

This section reviews some of the results from [11, 12], as they are needed in the following sections of the work. The problems considered here share the same initial geometry and boundary conditions, illustrated in Fig. 1, and differ only in the mechanical properties ascribed to the solid material. With a fixed coordinate system (X_1, X_2), a plane solid body occupying the region $0 \le X_1 \le B$ and $|X_2| \le B$ is considered. A half elliptic pit, given by $(X_1 / D)^2 + (X_2 / W)^2 = 1$ for $X_1 \ge 0$, is introduced on the surface $X_1 = 0$. The width and depth of this pit are chosen as $W = 10^{-3}B$ and $D = 0.1W$, respectively, as shown on the left part of Fig. 1. It should be mentioned, that pits of variable depths, D, and their influence on crack incubation have been considered in [11], but this issue will not be addressed in the present work. The boundary, which includes the surfaces $X_1 = 0$, $W \le |X_2| \le B$, and the surface of the pit, is denoted by Σ. This boundary is assumed to be in contact with a corrosive environment and to be initially covered by a passive film. The film is assumed brittle and characterised by its rupture strain, chosen as ε_f = 0.001. The material of the body is chosen to be either linear elastic or elastic-perfectly plastic, characterised by Young's modulus E = 206 GPa, Poisson's ratio ν = 0.3, and for plastic materials by the yield strength σ_y.

The body is considered to be in plane strain. The components of the boundary displacement and traction vectors are denoted by U_1 and U_2, and T_1 and T_2, respectively. The load is assumed to be applied in cycles and the components of the surface advance per load cycle due to material loss and of the current outward unit normal to the boundary are denoted by R_1 and R_2, and N_1 and N_2, respectively. The boundary conditions for one load cycle are

$$\begin{cases} T_1 = 0 \\ U_2 = -u \end{cases}, \quad \text{at } 0 \le X_1 \le B \text{ and } X_2 = -B \tag{1a}$$

$$T_1 = T_2 = 0, \quad \text{at } X_1 = B \text{ and } |X_2| \le B \tag{1b}$$

$$\begin{cases} T_1 = 0 \\ U_2 = u \end{cases}, \quad \text{at } 0 \le X_1 \le B \text{ and } X_2 = B \tag{1c}$$

$$\begin{cases} T_1 = T_2 = 0 \\ R_1 = -R\,N_1 \\ R_2 = -R\,N_2 \end{cases}, \quad \textbf{at } \Sigma \tag{1d}$$

where u is the applied peak displacement during the cycle, and R is the advance per cycle calculated via

$$R = R_d\,\varepsilon\,\theta(\varepsilon - \varepsilon_f) \tag{2}$$

In Eq.(2), ε is the surface strain and R_d is a rate parameter depending on the electrochemical conditions and load cycle type; for the physical reasoning behind Eq. (2) see e.g. [11]. The boundary displacement is chosen as $u = \varepsilon_f B$, which ensures a constant strain field in a rectangular body without surface flaws and is exactly on the threshold to break the protective film of the flat surface.

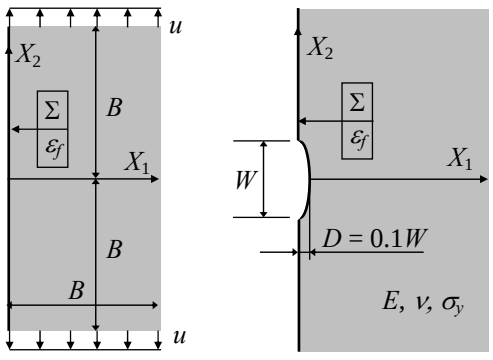

Fig. 1. Geometry of the moving boundary problems.

The described above geometry, material and boundary conditions constitute a moving boundary value problem (MBVP). This can be seen from the excess of boundary conditions along Σ, Eq. (1d), which compels the boundary to evolve in a way that the redistributed stresses are maintained in an instantaneous equilibrium with the applied loads. In the present context, each load cycle is understood as a new boundary value problem, with geometry determined by the entire past history of the evolving boundary. A numerical solution for the MBVP, based on a problem split into equilibrium and evolution sub-problems over each load cycle, is used. The equilibrium sub-problem is solved using the commercial finite element analysis program ABAQUS [13]. The surface strains, ε, obtained at equilibrium, provide the advance of the corroding surface Σ via Eq. (2). The evolution sub-problem is solved using an in-house procedure for surface tracking and geometry re-meshing. A thorough description of this procedure may be found in [14]. Thus the current geometry is changed and the finite element formulation of the boundary value problem for the next cycle is prepared.

For presenting results, a normalised load factor, σ_∞/σ_y, is introduced, where for the given boundary conditions the remotely applied stress is $\sigma_\infty = \varepsilon_f E / (1-\nu^2)$. A number of yield strengths, representing the range from elastic to very soft plastic materials, namely $0 \le \sigma_\infty/\sigma_y \le 0.5$, have been considered. The solutions of the corresponding moving boundary problems show that the surface of the initial pit evolves towards a crack-like shape and then grows as corrosion crack in the sense of deep slender notch [11,12]. An illustration of such evolution is given in Fig. 2, where results for the load factor $\sigma_\infty/\sigma_y = 0.15$ are collected in one. These are the profiles of the initial pit, the surface at crack incubation, and the crack at extension W. The crack extension, denoted by a, is measured from the initial pit surface to the current position of the crack tip, which with reference to the coordinate system in Fig. 1 is the point of largest X_1-coordinate along Σ. The incubation crack length is a_{inc}. The crack width in the tip region, denoted by 2ρ, is defined as the distance between the points where 45° lines running back from the crack tip intercept the crack faces.

The crack growth rate, da, is identified as the advance per load cycle of the crack tip point normalised with the electrochemical advance, i.e. $\mathrm{d}a = (R / R_\mathrm{d})_{tip} = \varepsilon_{tip}$. Fig. 3 shows the crack growth rate variation as a function of the square root of crack extension, normalised with the initial pit width W, for three chosen values of the yield strength, $\sigma_\infty/\sigma_y = 0$, $\sigma_\infty/\sigma_y = 0.15$, $\sigma_\infty/\sigma_y = 0.30$. Note, that the first value represents an elastic material.

As presented, the graph illustrates a clear separation between two stages of evolution that may also be distinguished on the fracture mechanical base. The stress intensity factor, K_I, for a sharp crack of length a, emerging from a surface pit with dimensional notations of Fig. 1, is

$$K_I = \sigma_\infty \sqrt{\pi a}\, f(a, D, W), \tag{3}$$

where $f(a, D, W)$ is a geometry factor, that may be found in e.g. [15]. The elastic solution for a deep slender notch with circular tip region of radius ρ (see [15]), provides an approximate value for the maximum strain at the tip

$$\varepsilon_{tip} = \frac{1-\nu^2}{E}\frac{2K_I}{\sqrt{\pi\rho}}, \tag{4}$$

where K_I is determined via Eq. (3). On the basis of this proportionality between K_I and the strain at the tip one concludes that there is a K_I–controlled zone surrounding the notch tip and the notch could be considered as a crack at sufficiently large length scale. In the considered case, $\varepsilon_{tip} = \mathrm{d}a$, and a linear relation between crack growth rate and the square root of crack extension in the results would also mean existence of a K_I–controlled zone surrounding the crack tip. An approximately linear relation between these two parameters is seen in the second stage of evolution in Fig. 3 for all materials shown. Therefore, the latter is called stage of K_I–controlled growth. The preceding stage is naturally called incubation. It is characterised by strain and dissolution localisation that lead to crack growth acceleration and eventual crack formation at the offset. Fig. 5 also shows that the crack extension at incubation, a_{inc}, is independent of the initial geometry and material yield strength, while the crack acceleration during propagation is clearly dependent on the material. Before turning attention to the latter observation, it is important to demonstrate the behaviour of the crack width. Fig. 4 shows the development of crack half-width, ρ, for the same materials as in Fig. 4. Because the graphs of the three evolutions are almost coinciding, they are given with solid, dashed and dotted lines, for $\sigma_\infty/\sigma_y = 0$, $\sigma_\infty/\sigma_y = 0.15$ and $\sigma_\infty/\sigma_y = 0.30$, respectively. The somewhat fuzzy behaviour of the crack width comes from the inaccuracy of the numerical determination of this parameter and has to be accepted. It must be noted, that during the incubation stage, the crack width is measured in the way described for propagating crack, unless the 45° lines running back from the tip do not yet intercept the pit faces. In this case the crack width, 2ρ, is set to the pit width, W. Hence, the curves in the stage of incubation start from the value $0.5W$, but are not entirely shown for convenience.

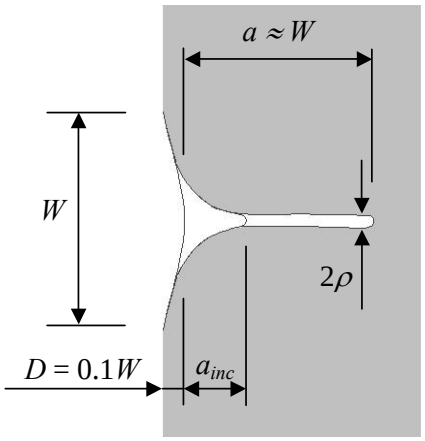

Fig. 2. Evolution of a corrosion crack geometry.

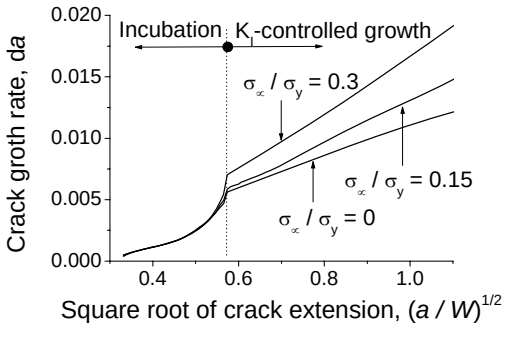

Fig. 3. Crack growth rate development.

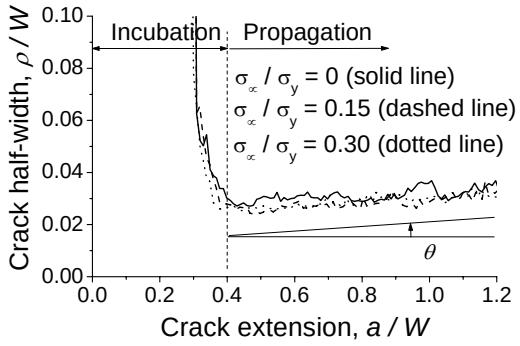

Fig. 4. Crack half-width development.

In spite of the numerical uncertainty introduced in Fig. 4, some solid observations could be made from the figure. Firstly, it shows again the independence of the incubation crack extension from the material yield strength. Secondly, the crack width attained at incubation is also found to be independent of the material yield strength and of the initial pit geometry. This is actually the instance where the evolving pit surface attains the smallest curvature at the tip during the entire evolution. Thirdly, the crack width during the propagation stage starts increasing slowly and nearly linearly. The rate of this increase is almost independent of the material properties, and is measured by the angle θ, that the crack face makes with the direction of propagation. As discussed in the next sections, the crack width increase is a consequence of the assumed model for surface advance, Eq. (2). It is characterised by corrosive blunting of the tip, which continues until the crack attains a shape allowing a steady-state growth, i.e. at constant rate da. During this growth the crack geometry is maintained self-similar, in such a way that all strains along the surface in the tip region are kept constant while that region expands as a void [11,12].

The crack growth rate attained at incubation and its development during propagation shows strong dependence on the material yield strength, Fig. 3. At the same time the crack width is independent of the material properties, Fig. 4. This suggests that shape changes of the crack tip region occur. To demonstrate the extent of these changes an appropriate scaling factor based on the elastic solution for a long slender notch is used. Using Eqs. (3) and (4) with $\sigma_\infty = \varepsilon_f E / (1-\nu^2)$, one can define a dimensionless shape factor by

$$\phi = \alpha \frac{\mathrm{d}\, a}{\varepsilon_f} \sqrt{\frac{\rho}{a}}\,, \tag{5}$$

where $\alpha = 1 / (2 f)$ is a factor depending on the geometry through $f(a, D, W)$. For an edge crack, emerging from a pit with dimensions of Fig. 1, $\alpha \approx 0.4458$ [15]. Note from Eq. (4), that $\phi = 1$ if the notch has exactly circular tip shape and the material is elastic. Note also that for a given yield strength, ϕ is proportional to the slope of the corresponding line in Fig. 4 representing crack propagation stage.

The dependence of the shape factor on the yield strength is presented in Fig. 5. The graph shows that the material yield strength is a parameter controlling the shape of the formed crack tip region. For elastic and very hard plastic materials, this region may be thought of as circular, and changes towards probably an ellipse with decreasing yield strength. The precise shapes, however, cannot be determined only on the base of the crack tip strain. An analysis of the surface strain distribution over the crack faces is needed.

3. Analysis of a steady state corrosion crack

The maximum strain at the tip of a long slender notch with circular tip, Eq. (4), is determined from the analytical solution for the strain field surrounding the tip of an elliptic hole [16]. This analytical solution is only approximately valid for the close vicinity of the tip, where the differences between the ellipse and the osculating circle are small in terms of curvature. Here the surface strain distribution along the entire curved part of the tip and not only the foremost point is essential. Therefore, numerical solutions for a long slender notch with half circular tip have been performed to demonstrate an interpretation of the results from the previous section. Finite element analysis is used. A large body with a long crack of

parallel walls and a circular tip region is considered. A standard boundary layer formulation of the problem is utilised. The layer is a circular region surrounding the crack tip and centred at the tip. The radius of the tip is ρ, while the radius of the boundary layer is taken to be $r = 100\rho$. This is considered sufficient for the K_1-terms in the expansions of stress, strain and displacement fields to dominate at the circular boundary, r, of the layer.

The geometry of the crack tip region is shown in Fig. 6, together with the coordinate system that will be used. Before continuing with the problem formulation and solution, the conditions of strain necessary to maintain the geometry of Fig. 6 self-similar during propagation, i.e. the conditions for steady-state growth parallel to X_1, are considered. Geometrically, steady-state growth implies that the X_1-component of the advance of every point along the crack surface should be the same and equal to the advance of the crack tip, denoted as before by da. For an arbitrary surface point n on the circular part of the tip, this means that the necessary advance, dn, normal to the surface is given by

$$\mathrm{d}\,n = \mathrm{d}\,a\cos\varphi = \mathrm{d}\,a\left(1+\frac{X_1}{\rho}\right), \tag{6}$$

using the notations of Fig. 6. On the upper and lower parallel straight crack surfaces the advance disappears. The linear model given by Eq. (2) yields dn / da = $\varepsilon / \varepsilon_{tip}$, where ε is the strain at the point n. Hence, Eqs. (2) and (6) require a distribution of surface strains that is given by

$$\varepsilon = \varepsilon_{tip}\left(1+\frac{X_1}{\rho}\right) \tag{7}$$

Since the profiles of longer cracks resemble the geometry depicted in Fig. 6, the aim here is to examine how well the strain field produced around the notch of Fig. 6 fulfils Eq. (7). Because the barrier posed by the rupture strain of the passive film, ε_f, is a lower limit strain, under which corrosion does not occur, the strain on the straight parts of the crack surfaces must be less than ε_f and equal to ε_f at the point where the straight and the half circular segments are connected, i.e. at $X_1 = -\rho$. This is a condition for the crack faces to stay parallel.

To find support for the suggested strain distribution, Eq. (7), finite element calculations have been carried out. The geometry of the boundary layer problem has been already described above. The material of the layer is again assumed to be elastic or elastic-perfectly plastic with properties as defined in the previous section. Plane strain conditions are considered and the load is applied via prescribed displacements along the circular boundary of the layer. Only the K_1-terms in the expansions for the displacements are taken. The analysis is performed using six-node triangular finite elements with quadratic interpolation in ABAQUS.

The surface strain distribution for three cases $K_\mathrm{I} / (\sigma_y \sqrt{\rho}) \le 0.88$, $K_\mathrm{I} / (\sigma_y \sqrt{\rho}) = 2.8$ and $K_\mathrm{I} / (\sigma_y \sqrt{\rho}) = 4.2$ is shown in Fig. 7 (these correspond to $\sigma_\infty / \sigma_y = 0$, $\sigma_\infty / \sigma_y = 0.10$ and $\sigma_\infty / \sigma_y = 0.15$, respectively). The distribution is given as a function of the X_1-coordinate, normalised width the crack width ρ. For convenience in comparison, the surface strain is also normalised using the form and notations of Eq. (5). Thus, the graph shows the variable

$$\varepsilon^* = \frac{\varepsilon E\sqrt{\pi\rho}}{2\left(1-\nu^2\right)K_\mathrm{I}}. \tag{8}$$

In the figure, ε_b^* denotes the normalised strain at the border between the flat crack face and the circular tip region. Note, that the normalised strain at the tip in elastic material should be unity, $\varepsilon_{tip}^* = \phi = 1$. There is a small discrepancy between this value and the numerical result in Fig. 7, because Eq. (4) is a result of a solution for elliptic hole, which approximates the actual strain at the tip for the considered long slender notch with parallel walls.

Fig. 7 shows a (nearly) linear distribution of surface strains for the case of elastic material, which supports the observation that the steady-state solution has a shape close to the one given in Fig. 6. The threshold strain is $\varepsilon_b^* = 0.2334$ read from Fig. 7. Now, we are provided with the necessary prerequisites to calculate the crack half width, ρ. The conclusion, considering Eq. (8), is that

$$\rho = 0.057\left(\frac{K_\mathrm{I}}{\varepsilon_f E}\right)^2. \tag{9}$$

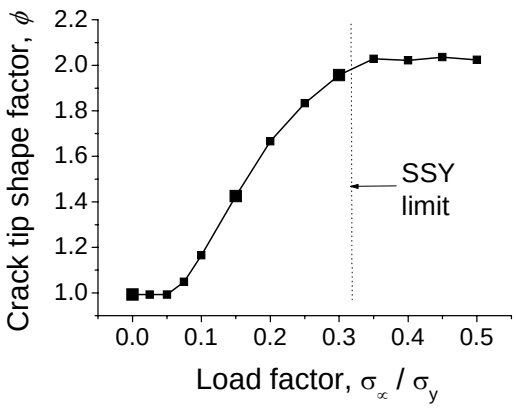

Fig. 5. Shape factor vs. yield strength.

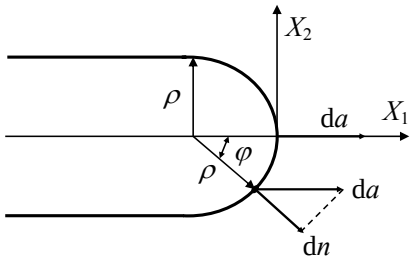

Fig. 6. Long plane notch with circular tip.

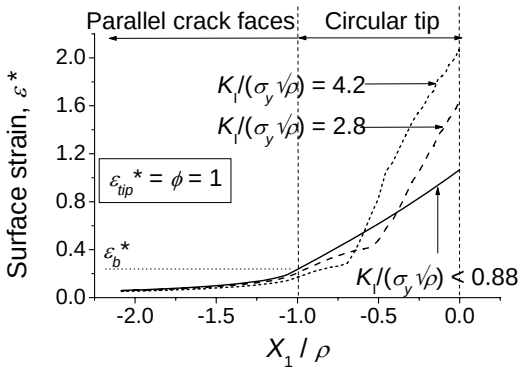

Fig. 7. Surface strain distributions for steady statecorrosion crack.

The crack width increases with increasing K_I, e.g. for an edge crack where K_I is proportional to $\sqrt{a}$, the crack width becomes proportional to a, meaning that the straight parts of the upper and lower crack surfaces form an angle. It becomes obvious, that a small value of remote load, as compared with $\varepsilon_f E$, maintaining a small angle between the crack surfaces is a prerequisite for the present steady-state analysis.

Another noteworthy detail is that the relation between the strain at the tip and the threshold strain is maintained at $\varepsilon_{tip}^* / \varepsilon_b^* = 4.56$ for the lowest load. Hence, the crack growth rate at steady-state is given by

$$\mathrm{d}a = \varepsilon_{tip} = \left(\varepsilon_{tip}^* / \varepsilon_b^*\right)\varepsilon_f = 4.56\,\varepsilon_f \qquad (10)$$

Opposed to crack growth in general, the growth rate is independent of remote load as long as the load is sufficiently small. Fig. 7 shows that plasticity leads to a distribution of surface strains that increases the corrosion rate in the vicinity of the tip and decreases the rate close to the border as compared to elastic material. The analysis does not allow a definite description of the surface shape, judging from strain distribution alone. However, a comparison based on the case with the largest scale of plasticity, $K_I / (\sigma_y \sqrt{\rho}) = 4.2$, of the maximum strain at the tip shown in Fig. 7, $\varepsilon_{tip}^* = 2.07$, and the one shown in Fig. 5, $\varepsilon_{tip}^* = 1.42$, suggests a trend. Seemingly because the solution for circular tip geometry provides a larger strain at the tip, the growing crack at a higher load have smaller curvature in the tip region, i.e. the corrosion crack is more blunted, in the sense of corrosion-induced blunting, in plastic material compared to elastic material.

4. Discussion and conclusions

The aim of the present work was to review previous and present some new results on nucleation and propagation of fatigue corrosion cracks as well as to examine them with the help of analysis of stationary corrosion cracks. The results presented, are solutions of moving boundary value problems. These arise from the evolutionary character of the corrosion crack initiation and growth as smooth surface advance cased by material loss. In the model for surface advance [11,12], it is accepted that deformation causes rupture of an existing passive film, but neither the dissolution rate of the uncovered bare metal nor the rate of repassivation are regarded as deformation dependent. The result of these simplifications is the linear relation between surface strain, Eq. (2). Despite some insufficiencies of the physical model suggested, the results presented in section 2 show the importance of the deformation-corrosion interaction for strain and dissolution localisation during crack incubation. The end of incubation is marked by the appearance of a K_I-controlled zone surrounding the crack tip. As examined in section 3, the shape of the formed crack tip is either close to circular for elastic and very hard plastic materials or more complex, but necessarily more blunted for softer plastic materials. This is a consequence of the linear model for surface advance. The subsequent growth under K_I-control is characterised by almost linear increase of the crack growth rate. The deviation from linearity, expected on theoretical grounds, is due to the increase of the crack width. This increase is a consequence of the advance threshold posed in the model by the rupture strain of the passive film. The crack width is found to depend linearly on the crack extension and this was also characterised in section 3.

The behaviour predicted on the basis of the linear model is not confirmed categorically by the appearance of corrosion cracks. In these cases one observes an established crack width that has been maintained nearly constant for a long period of growth. There are several physical reasons that have not been taken into account in the model but might affect the real behaviour. For example, in the case of inter-granular corrosion cracking in stainless steels the grain boundary (inter-phase) thickness limits from above the crack width. The Cr-rich grains could be regarded as non-dissolving, while the Cr-depleted inter-phase is susceptible to corrosion. The situation might be described as a tunnel-like area where the crack is allowed to grow. If a crack of width originally smaller

than the inter-phase thickness is evolving in the tunnel according to the model prediction, the grains will block the continuous width increase at some point of the evolution. After that, the grains could be regarded as a barrier for surface advance that replaces ε_f.

A prospect to further develop the model is to better describe the dissolution rate, R_d, presently assumed constant. Firstly, the bare surface dissolution rate, R_d, is altered in a stressed solid [17]. Secondly, during crack nucleation and propagation the transport processes in the corrosive environment, e.g. diffusion and electro-migration, lead to a distributed chemistry composition in the cavity, see e.g. [18]. This causes variation of the dissolution driving force and hence the dissolution rate along the cavity depth. The difficulty arising here is that the driving force variation depends on the current crack geometry and has to be found as a solution of a separate and more complex moving boundary problem. Nevertheless, this line of future work might be the most fruitful for model improvement.

References

[1] Olsson C-OA, Landolt D. Passive films on stainless steels – chemistry, structure and growth. Electrochim Acta 2003; 48(9): 1093-1104.

[2] Macdonald DD, Urquidi-Macdonald M. A coupled environment model for stress corrosion cracking in sensitised type 304 stainless steel in LWR environments. Corros Sci 1991; 32(1): 51-81.

[3] Laycock NJ, Newman RC. Localised dissolution kinetics, salt films and pitting potentials. Corros Sci 1997; 39(10-11): 1771-1790.

[4] Engelhardt G, Macdonald DD. Estimation of corrosion cavity growth rate for predicting system service life. Corros Sci 2004; 46(5): 1159-1187.

[5] Turnbull A. Modelling of environment assisted cracking. Corros Sci 1993; 34(6): 921-960.

[6] Ford FP. Quantitative Prediction of Environmentally Assisted Cracking. Corrosion 1996; 52(5): 375-395.

[7] Broberg KB. Cracks and fracture. Cambridge: Academic Press, 1999.

[8] Jivkov AP. Fatigue corrosion crack extension across the interface of an elastic bi-material. Eng Fract Mech 2004; 71(7-8): 1119-1133.

[9] Jivkov AP, Ståhle P. Strain-driven corrosion crack growth: A pilot study of intergranular stress corrosion cracking. Eng Fract Mech 2002; 69(18): 2095-2111.

[10] Kussmaul K, Blind D, Läpple V.. New observations on the crack growth rate of low alloy nuclear grade ferritic steels under constant active load in oxigenated high-temperature water. Nucl Eng Des 1997; 168: 53-75.

[11] Jivkov AP. Evolution of fatigue crack corrosion from surface irregularities. Theor Appl Fract Mech 2003; 40(1): 45-54.

[12] Jivkov AP. Surface irregularities as sources for corrosion fatigue. In: Mesomechanics of computation and design of use-specific materials. Sih GC, Sakai S, Panin VE, editors. Tokyo University Press, 2003, 184-191.

[13] ABAQUS User's Manual, Version 6.3, Hibbitt, Karlsson & Sorensen Inc., 2002.

[14] Jivkov, A.P. A moving boundary model for fatigue corrosion cracking. In: Moving Boundaries VII. Mammoli AA, Brebbia CA, editors., 2003, 55-64.

[15] Tada H, Paris PC, Irwin GR. The stress analysis of cracks handbook. New York: ASME Press, 2000.

[16] Creager M, Paris PC. Elastic field equations for blunt cracks with reference to stress corrosion cracking. Int J Fract Mech 1967; 3: 247-252.

[17] Devanathan MAV, Fernando MJ. Kinetics of charge transfer at mechanically strained copper electrodes – I. Anodic dissolution. Electrochim Acta 1970; 15: 1623-1636.

[18] Sharland SM. A mathematical model of the initiation of crevice corrosion in metals, Corros Sci 1992; 33(2): 183-201.